

Influence of oxide films on primary water stress corrosion cracking initiation of alloy 600

J. Panter ^{a,1}, B. Viguier ^{b,*}, J.-M. Cloué ^a,
M. Foucault ^a, P. Combrade ^a, E. Andrieu ^b

^a *Framatome, Centre Technique, BP 181, 71205 Le Creusot cedex, France*

^b *Centre Inter-Universitaire de Recherche et d'Ingénierie des Matériaux (CIRIMAT), CNRS/INPT/UPS, ENSIACET, 118 Route de Narbonne, 31077 Toulouse cedex 04, France*

Received 3 February 2005; accepted 5 October 2005

Abstract

In the present study alloy 600 was tested in simulated pressurised water reactor (PWR) primary water, at 360 °C, under an hydrogen partial pressure of 30 kPa. These testing conditions correspond to the maximum sensitivity of alloy 600 to crack initiation. The resulting oxidised structures (corrosion scale and underlying metal) were characterised. A chromium rich oxide layer was revealed, the underlying metal being chromium depleted. In addition, analysis of the chemical composition of the metal close to the oxide scale had allowed to detect oxygen under the oxide scale and particularly in a triple grain boundary. Implication of such a finding on the crack initiation of alloy 600 is discussed. Significant diminution of the crack initiation time was observed for sample oxidised before stress corrosion tests. In view of these results, a mechanism for stress corrosion crack initiation of alloy 600 in PWR primary water was proposed.

© 2005 Elsevier B.V. All rights reserved.

PACS: 62.40.M; 28.41.T; 82.80.M

1. Introduction

The intergranular stress corrosion cracking (IGSCC) of alloy 600 steam generator tubing is a problem of great importance in pressurised water reactors (PWRs). In spite of numerous studies

which have been worked out, the mechanisms that control IGSCC in this nickel based alloy are still under controversy. Besides, most of the mechanisms proposed, including corrosion enhanced plasticity model [1] (CEPM), oxidation-vacancies interactions [2] and creep [3], hardly account for crack initiation. Despite the differences which can exist between the mechanisms previously quoted, the properties of the oxides film (nature, protective aspect, brittleness . . .) always play an important role for all proposed mechanisms. It is also well known [4] that the shorter cracking time for alloy 600 and the maximum crack propagation rate are obtained under

* Corresponding author. Tel.: + 33 5 62 88 56 64; fax: + 33 5 62 88 56 63.

E-mail address: Bernard.Viguier@ensiacet.fr (B. Viguier).

¹ Present address: Laboratoire Matériaux et Procédés, EURO-COPTER, Aéroport Marseille/Provence, 13725 Marignane cedex, France.

electro-chemical conditions close to the Ni/NiO equilibrium potential. Considering all these facts, the aim of the present work was to perform a fine characterisation of the oxide scale developed in these particular experimental conditions, to investigate the consequences on the underlying metal and to test the influence of such a surface layers on primary water stress corrosion cracking (PWSCC) initiation of alloy 600.

2. Experimental details

Coupons of alloy 600, used for surface layers examination, have been extracted from a vessel head penetrator. The heat under concern denoted A below is known to exhibit quite a large sensitivity to crack initiation. Material used for stress corrosion tests is a steam generator tube labelled B also very sensitive to crack initiation. Chemical compositions of these two heats, as provided by the supplier, are given in Table 1.

Exposures were performed in simulated primary water (1200 ppm B, 2 ppm Li, deaerated) at 360 °C, 193 bar in a static autoclave. The hydrogen partial pressure was fixed at 30 kPa using a Pd–Ag membrane. A duration of 300 h was selected for the coupon exposures, this time corresponds approximately, for the heat A, to the mean cracking time of alloy 600 Reverse U-Bend (RUB) specimens tested under similar experimental conditions. These first specimens were discs (diameter: 25 mm, thickness: 1 mm) mechanically polished down to 1 µm diamond paste, washed, rinsed with deionized water and a Cl and S free solvent and finally dried. Stress corrosion tests and crack initiation time measurements were conducted using tube ovalized (TO) specimens [5], due to the smaller stress and strain applied as compared to RUB specimens. The specimens were grinded on their internal surface by removing 200 µm thick using a grind in alumina. Half of them were pre-exposed to primary water prior to the shaping of the TO (ovalization of the tube). A duration of 600 h was selected for the pre-oxidation, this time corresponds approximately,

for the heat B, to 3/4 of the mean cracking time of TO specimens tested under similar experimental conditions. Crack initiation and growth was followed by a reverse DC potential drop technique which is commonly used in high temperature environments [6].

Morphology and microstructure of the oxide films were investigated using a field emission gun scanning electron microscope (FEG-SEM) LEO 1530 operating at voltages from 100 V to 30 kV. Chemical analysis were performed in the SEM with an energy dispersive X-ray spectroscopy (EDX) system (Oxford Inca Energy). During the analysis accelerating voltage was set at 20 kV and the specimen current at 400 pA. Transmission electron microscope (TEM) characterisation and EDX analysis were performed on cross-section specimens obtained using the usual route as previously described [7]. A Jeol JEM 2010 from the TEM-SCAN service of the Paul Sabatier University, Toulouse and a Philips ‘Tecnaï 20 F’ in the electronic microscopy laboratory of EDF research centre ‘Les Renardières’ were used, both operating at 200 kV. In addition, chemical analysis located in the first microns just beneath the oxide scale were performed in the SEM on TEM cross-section specimens in order to take advantage of the small thickness of the TEM specimens and of the electron beam characteristics of the FEG-SEM in order to reach a better spatial resolution in terms of EDX analysis.

Local determination of chemical composition was performed using secondary ions mass spectrometry (SIMS) from CAMECA IMS4F/6F. Depth profile mode was selected on the SIMS with an analysed zone diameter of 30 µm whereas the total area of the abrasion zone was 150 × 150 µm². The abrasion rate was measured to be 3.5 Å s⁻¹ due to an abrasion current of 10 nA. Cs⁺ ions were used in order to reduce the matrix effect. Chemical composition of metallic species were calculated by normalising the different signals assuming that the last points of the profiles correspond to the bulk alloy composition [8], which allows to plot mass composi-

Table 1
Chemical composition of the materials used in this study (wt%)

Element	Ni	Cr	Fe	C	Mn	Si	S	P	Co	Al	Ti
A	73.8	16.05	8.8	0.058	0.81	0.45	<0.001	0.007	0.04	0.24	0.29
B	73.8	16.07	8.39	0.034	0.83	0.26	0.001	0.011	0.018	0.23	0.25

tion versus abrasion time or depth (note that in this procedure oxygen was not normalised and arbitrary units are used). However this usual technique does not allow a precise determination of the thickness of the different layers, this is due mainly to the roughness of the oxide scale and of the interfaces. This roughness is often accentuated by the different rate of abrasion of oxide and metal which does not allow preventing the mixing of ions coming from remaining oxide islands and ions coming from the underlying alloy. Consequently a new procedure was designed in order to detect much more precisely the transition between different layers and the localisation of species beneath the oxide scale. This procedure which can be called 'reversed profile' consists in starting the abrasion from the metal towards the oxide scale. This necessitates the preparation of a specific thin specimen by mechanical polishing. Since abrasion starts from the polished surface, which eliminates the roughness problem, this procedure reveals very sharply the composition changes when crossing an interface. It also allows a much more accurate measurement of scale thickness, and in the case of oxidised samples it uniquely allows the detection of oxygen atoms in the metal underneath the oxide. The dedicated specimens were prepared using the following way: the oxidised face of the coupon was glued on a cylindrical rod (diameter: 30 mm, height: 20 mm) made of copper. The coupon was then mechanically polished on the alloy side down to a thickness of less than 10 μm . A final polishing was done using a colloidal silica suspension (OP-S Suspension™ Struers). Finally the ensemble was cut to fit SIMS specimen size: $3 \times 7 \times 1 \text{ mm}^3$. For this experiment the abrasion rate was experimentally measured to be 7 \AA s^{-1} due to the use of an ionic abrasion current of 20 nA.

3. Results

3.1. Structure of the oxide layer

On Fig. 1, plane SEM micrograph of the oxide film developed on alloy 600 in PWR simulated primary water is shown. The external oxide scale seems not to be compact but instead to be constituted of separated crystallites which define two families according to their size. The first family is made of small crystallites with an average size close to 50 nm and covers the major part of the specimen surface, while the second one is made of larger crystallites (size equal or greater than 200 nm) that

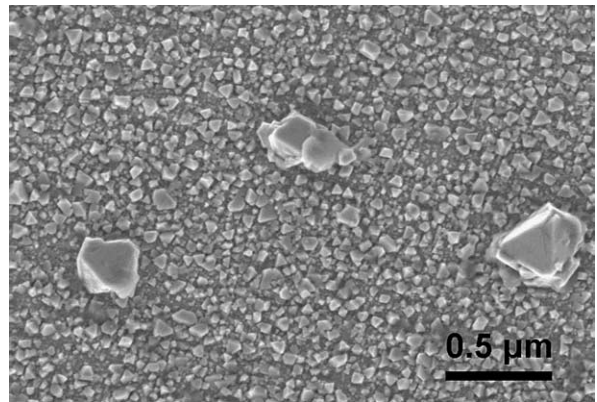


Fig. 1. SEM plane view of the oxide film after exposure 300 h at 360 °C in PWR simulated primary water, showing two families of oxide crystallites forming a non-continuous layer.

spread rather homogeneously on the specimen surface. The non-compact character of the external oxide layer is also revealed by TEM observation of cross-section specimens as shown in Fig. 2. The average thickness is about 70 nm, while the thickness of the layer appears to be heterogeneous due to different crystallite sizes which range from 50 to 200 nm (which corroborates the SEM observations). Crystallographic nature of large oxide crystallites was also investigated by using electron diffraction (Fig. 2) which allowed with TEM–EDX analysis to identify the crystallites as spinel oxides of the type NiFe_2O_4 . Below the outer oxide layer, a very thin 'fuzzy' layer is observed as indicated by white arrow

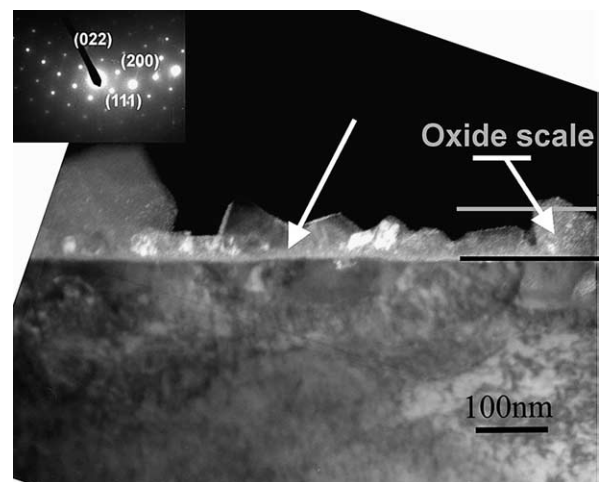


Fig. 2. TEM cross-section of the oxide film. The diffraction pattern inserted was taken from the large grain on the left and is indexed according to the spinel structure.

on Fig. 2. The thickness of this layer ranges around 10 nm but seems to be quite constant and moreover the layer looks compact and continuous. The external oxide crystallites seems to be embedded in this layer.

3.2. Composition variations

The variations of elemental composition have been established on the oxide scales and the underlying metal for the metallic species and for the penetration of oxygen in the metal. Chemical composition (wt%) in nickel, chromium and iron as measured by EDX in the FEG-TEM are plotted versus the distance from the outer surface. The oxide layer is enriched in iron on the outer part of the oxide film and mainly composed of chromium in the inner part. It is worth noting that the measured chromium content (70 wt%) must be considered as a lower limit, due to the precision of the technique and the possible tilt of the scale versus the electron beam. Actually a quasi pure chromium oxide could be identified in what was described above as a very thin ‘fuzzy’ layer. Chemical analysis made in the underlying metal revealed a chromium depletion. Unfortunately, the analysed profile shown in Fig. 3 had to be stopped before the end of the Cr depleted zone because the foil thickness increased too rapidly leading to erroneous measurements of nickel and chromium contents due to fluorescence effects. Several composition profiles obtained by TEM–EDX indicate that the minimum

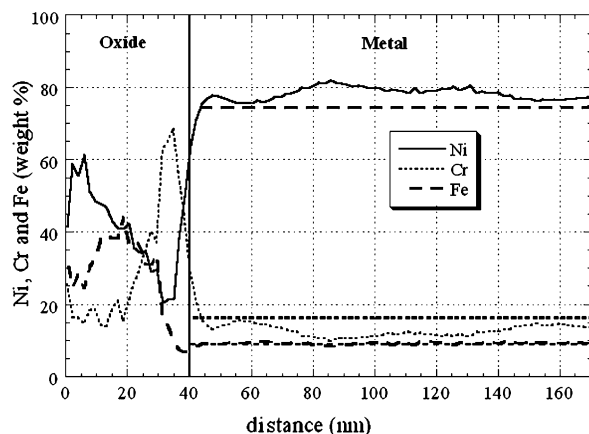


Fig. 3. Composition profile in Ni, Cr and Fe as a function of the distance as measured by EDX analysis in a FEG-TEM. The horizontal lines show the nominal composition of the alloy.

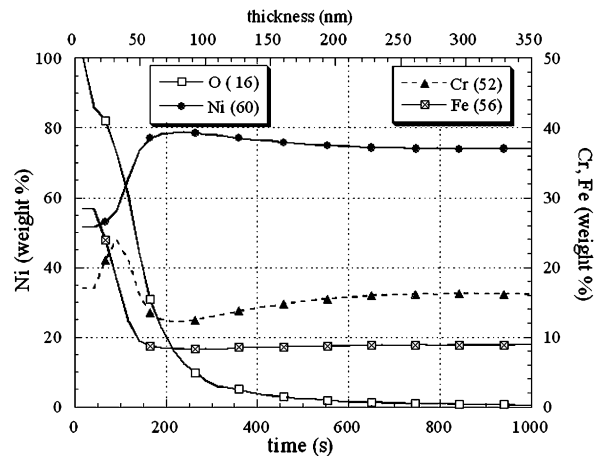


Fig. 4. Composition profile measured in the SIMS, starting the abrasion from the outer surface to the metal (arbitrary units are used for oxygen signal).

chromium concentration can reach values as low as 5% and the depth of the depleted zone was measured to be approximately two times the average thickness of the oxide scale, i.e. 140 nm.

These EDX measurements are confirmed by SIMS profiles as shown in Fig. 4, that is: a strong enrichment in iron at the oxide outer surface, a chromium rich inner layer and a chromium depleted zone. The oxygen signal seems to indicate some penetration of oxygen under the oxide layers. However, as presented in Section 2, the abrasion from the surface in the SIMS, associated with the large area which is analysed results in smoothing the composition profiles. Thus, ‘reversed profiles’ have been carried out, starting the abrasion from the underlying alloy (a flat surface) towards the oxide surface, in order to measure more precisely oxygen and oxide distribution at the vicinity of the oxide-metal interface. Fig. 5 shows the results corresponding to such analysis conditions for the following selected ions O^- , NiO^- , CrO^- and FeO^- . Black arrows have been added to the curves to point out different interfaces revealed by the sudden increase of the different signals. When dealing with oxide piling sequence, these profiles confirm what was yet known in terms of thickness and chemical compositions. However, surprisingly, the first ionic signal to increase is identified as oxygen alone without any correlation with other signals. The extent of this zone where oxygen penetrates beneath the oxide reaches 100 nm.

The backscattered electrons SEM micrograph presented in Fig. 6, taken on TEM cross-section, shows a rather surprising image contrast located

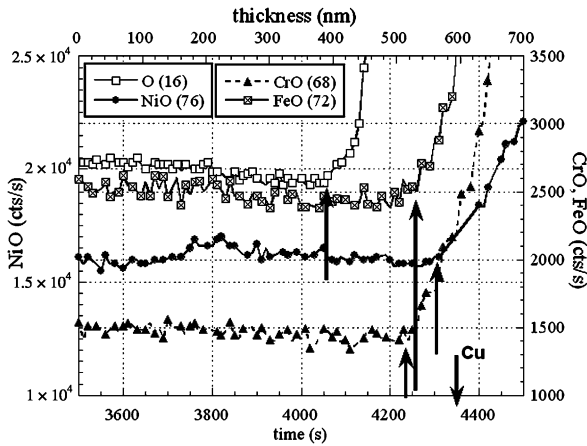


Fig. 5. ‘Reversed profile’ obtained in the SIMS under the oxide scale (the abrasion started from the metal to the surface, see Section 2), the arrows indicate the rising of signal, marking the edge of the different layers.

in a triple grain boundary of alloy 600. The associated chemical analysis of this area, based on EDX line scans, reveals a local enrichment in chromium together with oxygen. Carbon is not detected in this area so that this contrast cannot be associated with chromium carbide. This defect is located at a dis-

tance from the oxide-alloy interface which is close to 3 μm .

3.3. Stress corrosion cracking test

Stress corrosion tests have been carried out, for the alloy B, on TO specimens at 360 °C in simulated primary PWR water, the results of the present study have been compared to the large number of experiments previously performed in the laboratory for the same heat. In such conditions, initiation of cracks occurs repeatedly after 700–1000 h of exposure. The exposure is then maintained in order to let the cracks open and grow. Fig. 7 presents an example of SEM micrograph of a crack observed on a TO specimen after 1800 h of exposure. This kind of cracks was observed systematically on TO specimens exposed to such conditions. Two grinded tubes were submitted to a pre-exposure treatment consisting of 600 h in simulated PWR water at 360 °C under 0.3 bar of hydrogen. The tubes were then tested with the usual route, that is shaped to TO specimens and exposed again. When such a pre-exposure was done, the crack initiation time is strongly reduced, dropping to 350 and 450 h for the two specimens tested. This experiment clearly

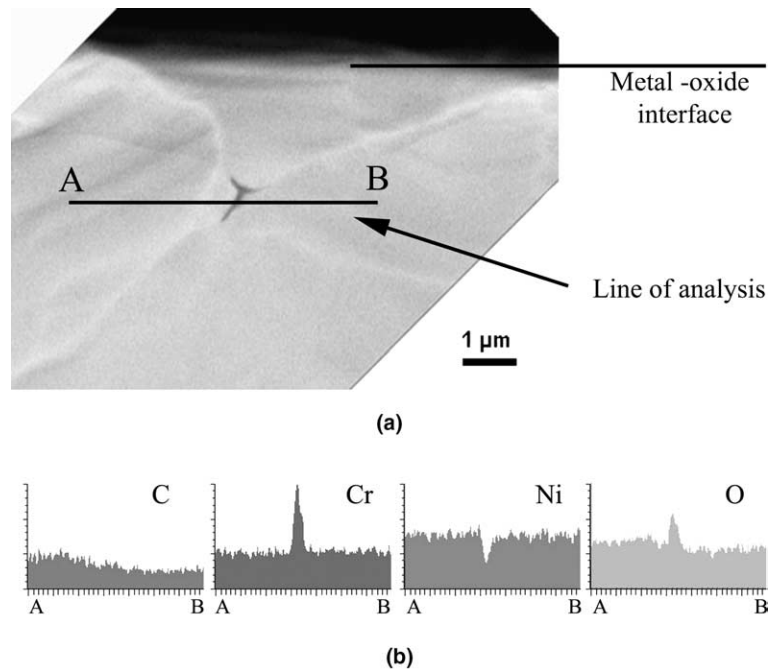


Fig. 6. Backscattering electron FEG-SEM micrograph (a) showing a contrast associated to a triple grain boundary 3 μm down the surface. The profile of EDX analysis across that triple grain boundary shown in (b) indicate that this contrast may arise from a chromium oxide and not from a carbide.

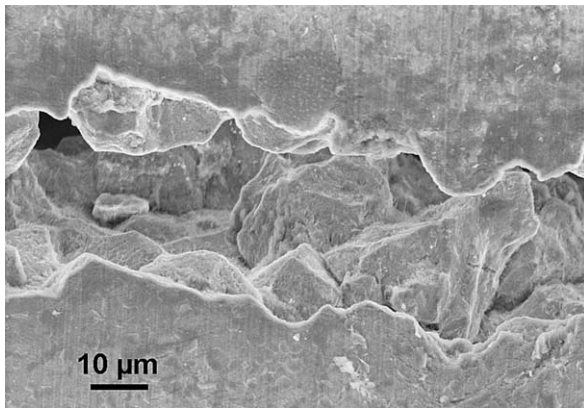


Fig. 7. SEM micrograph of a SCC crack after 1800 h exposure.

showed that pre-exposure period, even if out of stress, reduces significantly the crack initiation time.

4. Discussion

The first finding of the present study concerns the structure of the oxide layer which develops over Alloy 600 during the corrosion in high temperature water. The outer oxide scale which is observed is made of two families of grains, in agreement with what was reported in previous studies [9]. The first family is composed of discrete large crystallites, which were found to be spinel oxides of the type NiFe_2O_4 . The second one which apparently covers the entire surface, and whose crystallites are at least two times smaller, was found to be made of grains of a mixed oxide of nickel, chromium and iron. The non-compact character of the oxide scale made of mixed oxides is evidenced so that its ability to play a significant role in terms of alloy protection is questionable. This observation could bring some credits to a mechanism of growth involving dissolution and precipitation in order to explain the observed microstructure. Moreover, a very compact inner layer of about 5 nm thick is also evidenced by TEM (the ‘fuzzy’ layer). This thin layer, made of chromium oxide, is located at the interface between the oxide grains and the alloy, it is thus the first continuous layer which is really able to play the role of barrier layer. This last information is very important, and changes the usual description of the corrosion scales, in agreement with more recent observations in a similar alloy [10]. Up to now the oxide formed on stainless steels, or on nickel–chromium alloys, in hot water, was considered as a duplex layer, formed only by spinel oxides [9,11].

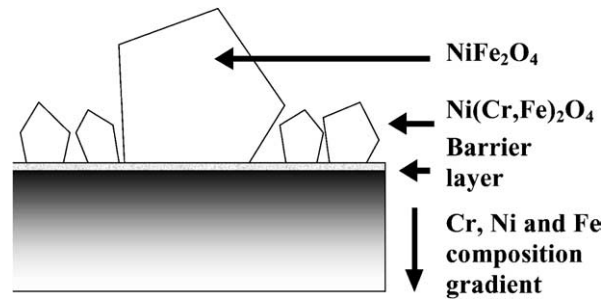


Fig. 8. Sketch of the oxide film and consequences on the underlying metal. The barrier layer is composed of chromium oxide.

By contrast, according to the present observations the oxide scale should be described as a triple layer as summarised in the sketch presented on Fig. 8.

One also must take attention to the consequences of the corrosion on the underlying metal, that is the presence of a chromium depleted layer. The thickness of this layer (140 nm) is close to twice the oxide film thickness and the chromium concentration can drop down to 5 wt%. In the literature, it is well known, at least for high temperature experiments, that nickel–chromium alloys are sensitive to internal oxidation and intergranular oxidation when the concentration in chromium becomes lower than 10% [12]. So chromium content in the affected zone is probably a crucial parameter which might account for the sensitivity to IGSCC in 360 °C primary water, of alloy 600. The formation of the chromium depleted zone must be related to the presence of the chromium oxide layer. Chromium containing alloys may form such a continuous chromium oxide layer provided their chromium content is higher than about 15%. The layer can form either by selective oxidation of other compounds of the alloy (Fe, Ni) or by the diffusion and selective oxidation of chromium [13]. The former case is not thought to happen since it would not lead to any change in chemical composition of the alloy beneath the oxide. Since a chromium depletion is observed, we believe that chromium rich layer is formed by the later mechanism, that is the diffusion and selective oxidation of chromium atoms. Simonen et al. [14] studied such oxidation mechanism and showed that it implies the injection of vacancies in the material under the oxide layer.

Another feature concerns the presence of oxygen in the metal under the oxide scale. Oxygen has been observed in two instances. First, the ‘reversed profiles’ performed by SIMS show an increase

of oxygen signal well before reaching the oxide (Fig. 5). This oxygen enrichment is not related to the formation of any oxide of the metals present in the matrix (CrO nor NiO) and thus may correspond to oxygen atoms dissolved in the metal matrix. The width of the oxygen enriched layer corresponds roughly to the chromium depleted zone observed by EDS. Secondly oxygen was observed on a triple grain boundary by EDS analysis. In this case, oxygen is correlated to a strong increase of chromium content, that is the feature observed in Fig. 6 certainly corresponds to a chromium oxide precipitate. It is worth noticing that such an oxide was never observed on sample before corrosion exposure, so that it is believed that this oxide formed during the stay in primary water. This oxide which grew three micrometers under the metal surface indicates that oxygen can be transported over such large distances. Such intergranular penetrations were already reported [15], but it remains difficult to understand how oxygen was able to diffuse so fast in this material, in these electro-chemical conditions at this temperature. Indeed, by extrapolating at 300 °C the results of Bricknell and Woodford [16] and Iacocca and Woodford [17], on the intergranular diffusion of oxygen in nickel at high temperature, a penetration of oxygen of 15 nm would take about ten years. Scott [18] emitted the assumption that under certain circumstances, related to the mechanical loading or to the porous structure of the cracks, the diffusion of oxygen can be widely accelerated as compared to the normal bulk diffusion coefficients. However these assumptions and simply any modelling of PWSCC of alloy 600 based on a mechanism of internal oxidation, is completely rejected by Staehle and Fang [19].

Finally we realised a decoupling between corrosion in primary water and applied stress. This decoupling aimed at being discriminating towards mechanisms proposed to explain PWSCC of nickel base alloys [2,20,21]. The tests realised on the casting B of alloy 600 mill-annealed evidenced a decrease of PWSCC initiation time for specimens pre-exposed without stress in primary water. As a consequence, these results contradict the theories asserting that a coupling between the applied stress and the defects, or other species, injected during growth of the oxides layers, is necessary to damage the material. On the contrary, it seems that the growth of the oxides layers developing in primary water can create by itself defects in the material. The weakening effect of a pre-exposure on nickel alloys is well known at

high temperature. In these conditions, the embrittlement is attributed either to the injection of vacancies due to the cationic growth of the oxides layers [22], or to the diffusion of oxygen in the grain boundaries [23]. In the first model, the vacancies that migrate to the grain boundaries participate to the growth of intergranular cavities and allow, when mechanical tests are realized at lower temperature, to accelerate a ductile intergranular damage of the material. This model does not seem to be applicable to alloy 600 exposed in primary water since in these cases, intergranular cavities were not observed [24]. Furthermore, the rupture of this alloy in primary water is brittle intergranular. In the second model proposed, the diffusion of the oxygen allows the formation of oxides in the grain boundaries and so contributes to their embrittlement. This second mechanism seems to explain better the decrease of the crack initiation time observed for pre-exposed specimens and is supported by the evidence of oxygen penetration under the oxide scale.

The ensemble of the previous findings can be easily conciliated by considering some binding effect between vacancies and oxygen atoms. Such binding have been evidenced recently in a study of the oxidation of pure nickel at high temperature [25,26]. As was pointed above, in the present study the selective oxidation of chromium produces vacancies close to the metal-oxide interface. Driven by concentration gradient these vacancies will diffuse towards the bulk of the material, essentially by the grain boundaries. The first effect of this migration of vacancies is an acceleration of the diffusion of chromium in the opposite direction accelerating the chromium depletion. Let us note that the chromium content profile predicted by this model (see Fig. 14 in [14]) compares very well with the profiles obtained in our study. The second effect of this migration of vacancies is that a transport of the interstitial species such as oxygen is expected by a binding effect between the vacancies and these atoms of small sizes. This effect is marked all the more as the temperature is low and the mobility of these couple is almost equal to that of the vacancies alone, which is much higher than the mobility of oxygen alone [27]. If we consider the concentration profiles of vacancies calculated in [14], we can then explain the observed penetrations of oxygen over very large distances. Such an oxygen penetration and the subsequent possible intergranular oxidation, can also occur during any corrosion treatment even without any load applied. This phenomenon is likely to be responsible

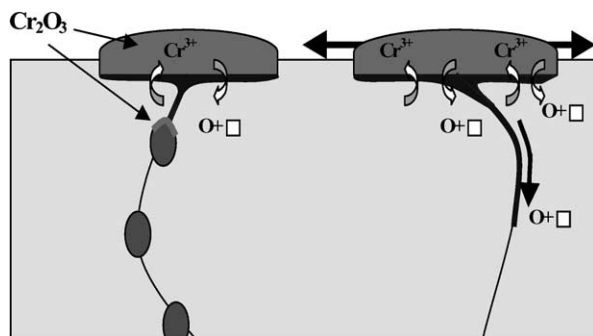


Fig. 9. Sketch summarising the growth of the chromium oxide layer accompanied by the injection of vacancies that transport oxygen. The benefic role of intergranular carbides reside in their role of trapping the oxygen as illustrated schematically.

for the decrease of the time of initiation of test specimens in mill-annealed pre-exposed alloy 600 B. As a consequence, all the results obtained in this study plead for a mechanism for initiation based on an embrittlement of the grain boundaries by internal oxidation [18,28,29]. The proposed mechanism is summarised in the sketch of the Fig. 9: the selective oxidation of chromium produces vacancies, these vacancies are bound with the oxygen atoms which they transport towards the metal along grain boundaries, thus weakening the boundaries. The positive effect of the presence of carbides at the grain boundary is also illustrated in Fig. 9, indeed these carbides may act as oxygen traps along the diffusion path, thus impeding the penetration of oxygen.

The proposed mechanism is in good agreement with previously established experimental facts, in particular:

- (i) The maximum sensitivity of alloy 600 to SCC initiation is observed near the Ni/NiO equilibrium. In these conditions, the oxide scale is destabilised and the damaging mechanism is maximised.
- (ii) The time to fracture t_F of alloy 600 specimens was found to depend on the applied stress [30] according to the relation: $t_F = k\sigma^{-4}$. The value -4 for the stress power can be readily rationalised noting that the fracture toughness under SCC conditions (K_{ISCC}) is a material characteristic and can be considered to be constant ($K_{ISCC} \propto \sigma\sqrt{\pi \cdot x} = \text{constant}$) and that if damage lies on a diffusional mechanism, the damaged length x can be written $x \propto B\sqrt{t}$.

Furthermore, by considering this type of mechanism, the sensitivity or the resistance to stress corrosion of other nickel base alloys can be anticipated. In particular, the good resistance of alloy 690 can be explained by its strong concentration in chromium which allows it to form quickly a protective chromium oxide layer. Only very small intergranular defects are then produced. To propagate the very small defects formed by the internal oxidation, very high stress would be needed. But as this material has only weak mechanical properties such high stress will not be retained by the material and the defects are not able to propagate. This mechanism may also apply for primary water stress corrosion cracking of alloy 718. Indeed, this alloy has an intermediate chromium content as compared to alloys 600 and 690. Considering the good resistance to crack initiation of polished samples of this alloy, its chromium content is high enough to allow the fast formation of a continuous chromium oxide layer. On the other hand when an intergranular defect is present at surface, its high mechanical properties allow to sustain sufficient stress to open the very weak part of grain boundary damaged in front of the defect, which explain why this alloy is sensitive to SCC propagation.

5. Conclusions

The corrosion products on alloy 600 specimens exposed to simulated PWR primary water (0.3 bar and 360 °C) have been characterised by electron microscopy (SEM and TEM) and chemical analysis (EDX and SIMS). It was shown that the oxide scale must be considered as a triple layer and that only a thin chromium oxide layer is continuous and may act as a barrier.

The analysis were also performed in the underlying metal and it was shown that there exists a chromium depleted zone in the metal and that oxygen penetrates over large distances the metal. Oxygen was observed in solution within this depleted zone and associated with chromium in a triple grain boundary as far as 3 μm from the oxidised surface. It is proposed that the selective oxidation of chromium produces vacancies that transport oxygen atoms in the metal leading to some intergranular oxidation. Such mechanism explains also why a pre-exposure without stress is able to decrease the SCC initiation time for approximately half of its value as we observed.

Acknowledgements

The authors are grateful to the French Nuclear Safety Authority for financial support.

References

- [1] T. Magnin, F. Foct, O. De Bouvier, Hydrogen effects on PWRSCC mechanisms in monocrystalline and polycrystalline alloy 600, In: Proc. of Ninth Int. Symp. On Environmental Degradation of Materials in Nuclear Power Systems-Water Reactors, Newport Beach (1999) 27.
- [2] E. Andrieu, B. Pieraggi, Oxidation-deformation interactions and effect of environment on the crack growth resistance of Ni-base superalloys, in: T. Magnin, J.M. Gras (Eds.), Corrosion-deformation Interactions, Nice, France Les éditions de physique, 1996, p. 294.
- [3] G. Was, D.J. Paraventi, J.L. Hertzberg, Mechanisms of environmentally enhanced deformation and intergranular cracking of Ni–16Cr–9Fe alloys, in: T. Magnin, J.M. Gras (Eds.), Corrosion-deformation Interactions, Nice, France Les éditions de physique, 1996, p. 410.
- [4] T. Cassagne, B. Fleury, F. Vaillant, O. De Bouvier, P. Combrade, An update on the influence of hydrogen on the PWSCC of alloy 600 in high temperature water, In: Proc. of Eighth Int. Symp. On Environmental Degradation of Materials in Nuclear Systems-Water Reactors, La Grange Park, Illinois (1997) 307.
- [5] R. Gate, B. Rassinoux, A. Gelpi, M. Le Calvar, B. Sala, Mechanical and Thermohydraulic Testing on Steam Generator Tubing Cracked in Laboratory Stress Corrosion, In: Proc. of Progress in the Understanding and Prevention of Corrosion, Barcelona, Spain (1993) 1542.
- [6] W.R. Catlin, D.C. Lord, T.A. Prater, L.F. Coffin, Automated Methods for Fracture and Fatigue Crack Growth ASTM STP 877 (1985) 67.
- [7] J. Panter, B. Viguier, E. Andrieu, Microstructure evolution of alloy 600 during dry oxidation, In: Proc. of Les Embiez 2000, Les Embiez, Trans Tech Publications (2001) 141.
- [8] D. Monceau, K. Bouhanek, R. Peraldi, A. Malie, J. Mater. Res. 15 (3) (2000) 665.
- [9] C. Soustelle, M. Foucault, P. Combrade, K. Wolski, T. Magnin, PWSCC of Alloy 600: A Parametric Study of Surface Film Effects, In: Proc. of Ninth Int. Symp. on Environmental Degradation of Material in Nuclear Power Systems-Water Reactors (1999) 105.
- [10] F. Carette, M.C. Lafont, G. Chatainier, L. Guinard, B. Pieraggi, Surf. Interface Anal. 24 (2002) 135.
- [11] S. Gardey, Etude de la corrosion généralisée des alliages 600, 690 et 800 en milieu primaire. Contribution à la compréhension des mécanismes, PhD Thesis, Université Pierre et Marie Curie (1998).
- [12] C.S. Giggins, F.S. Pettit, Trans. Met. Soc. AIME 245 (1969) 2495.
- [13] J. Robertson, Corros. Sci. 32 (1991) 443.
- [14] E.P. Simonen, L.E. Thomas, S.M. Brummer, Diffusion kinetic issues during intergranular corrosion of Ni-base alloys, In: Proc. of Corrosion 2000 (2000) 226.
- [15] T.S. Gendron, S.J. Bushby, R.D. Cleland, R.C. Newman, Oxidation embrittlement of alloy 600 in hydrogenated steam at 400 °C, In: Proc. of Eurocorr'96 (1997) M24.
- [16] R.H. Bricknell, D.A. Woodford, Scr. Metall. 30 (1982) 257.
- [17] R.G. Iacocca, D.A. Woodford, Metall. Trans. A 19 (1988) 2305.
- [18] P.M. Scott, An overview of internal oxidation as a possible explanation of intergranular SCC of alloy 600 in PWRs, In: Proc. of Ninth Int. Symp. On Environmental Degradation of Materials in Nuclear Power Systems-Water Reactors, Newport Beach (1999) 3.
- [19] R.W. Staehle, Z. Fang, Comments on a proposed mechanism of internal oxidation for alloy 600 as applied to low potential SCC, In: Proc. of Ninth Int. Symp. on Environmental Degradation of Material in Nuclear Power Systems-Water Reactors (1999) 69.
- [20] P.M. Scott, M. Le Calvar, On the role of oxygen in SCC as a function of temperature, in: T. Magnin, J.M. Gras (Eds.), Corrosion-deformation Interactions, Les éditions de physique, Nice, France, 1996, p. 384.
- [21] T. Magnin, A unified model for trans and intergranular stress corrosion cracking in fcc ductile alloys, in: T. Magnin, Gras, J.M. (Eds.), Corrosion-deformation Interactions, Fontainebleau, France, Les éditions de physique (1992) 410.
- [22] P. Hancock, Influence of vacancies produced by oxidation on the mechanical properties of nickel and nickel–chromium alloys, In: R.E. Smallman (Ed.), Vacancies '76 Met. Soc. (1976) 215.
- [23] R.H. Bricknell, D.A. Woodford, Metall. Mater. Trans. A 12 (1981) 425.
- [24] C.D. Thompson, H.T. Krasodonski, N. Lewis, G.L. Makar, Prediction of PWSCC in nickel base alloys using crack growth rate models, In: Proc. of Seventh Int. Symp. On Environmental Degradation of Materials in Nuclear Power Systems-Water Reactors (1995) 867.
- [25] S. Perusin, B. Viguier, D. Monceau, L. Ressler, E. Andrieu, Acta Mater. 52 (2004) 5375.
- [26] S. Perusin, B. Viguier, D. Monceau, E. Andrieu, Mater. Sci. Forum 461–464 (2004) 123.
- [27] R.A. Johnson, N.Q. Lam, Phys. Rev. B 13 (1976) 4364.
- [28] P. Berge, Corros. Sci. 10 (1970) 185.
- [29] T.S. Gendron, P.M. Scott, S.M. Brummer, L.E. Thomas, Internal oxidation as a mechanism for steam generator tube degradation, In: Proc. of Third Int. Steam Generator and Heat Exchanger Conference, Toronto, Canadian Nuclear Society (1998) 5.18.
- [30] R. Bandy, D. Van Rooyen, Corrosion-Nace 40 (1984) 425.